J. Chem. Thermodynamics 97 (2016) 191–205

Contents lists available at ScienceDirect

J. Chem. Thermodynamics

journal homepage: www.elsevier.com/locate/jct

Volumetric and acoustical properties of aqueous mixtures of N-methyl-2-hydroxyethylammonium butyrate and N-methyl-2-hydroxyethylammonium pentanoate at T = (298.15 to 333.15) K

Yang Li [a], Eduardo J.P. Figueiredo [b], Mário J. Santos [b], Jaime B. Santos [b], Nieves M.C. Talavera-Prieto [c], Pedro J. Carvalho [d], Abel G.M. Ferreira [c,*], Silvana Mattedi [e]

[a] Shanghai Key Laboratory of Modern Metallurgy & Materials Processing, Shanghai University, Yanchang Road, 200072 Shanghai, China
[b] Department of Electrical and Computers Engineering, University of Coimbra, Polo II, Rua Sílvio Lima, 3030-970 Coimbra, Portugal
[c] Department of Chemical Engineering, University of Coimbra, Polo II, Rua Sílvio Lima, 3030-970 Coimbra, Portugal
[d] CICECO, Departamento de Química, Universidade de Aveiro, 3810-193 Aveiro, Portugal
[e] Escola Politécnica, Universidade Federal da Bahia, Rua Aristides Novis 2, Federação, 40210-630 Salvador, Bahia, Brazil

ARTICLE INFO

Article history:
Received 4 November 2015
Received in revised form 23 January 2016
Accepted 29 January 2016
Available online 6 February 2016

Keywords:
Ionic liquid
Density
Pitzer–Simonson theory
Speed of sound
Apparent molar volume
Apparent molar isentropic compressibility

ABSTRACT

The speed of sound in the protic ionic liquids (PILs) N-methyl-2-hydroxyethylammonium butyrate (m2HEAB) and N-methyl-2-hydroxyethylammonium pentanoate (m2HEAP) was measured at atmospheric pressure, and over the range of temperatures T = (293.15 to 343.15) K. The speed of sound and density of aqueous mixtures of the ionic liquid were also determined throughout the entire concentration range, within the (298.15 to 333.15) K temperature range and at atmospheric pressure. The excess molar volume, excess isentropic compressibility, excess speed of sound, apparent molar volume and apparent molar isentropic compressibility were calculated from the experimental density and speed of sound values. Furthermore, all the properties were correlated with selected analytical functions. The apparent molar volume of aqueous PILs was analysed by Pitzer–Simonson theory. The speed of sound of the PILs was predicted with the Wu *et al.* model and the molar compressibility of the same PILs and their aqueous mixtures were calculated from Wadás model. The results demonstrate that the molar compressibility calculated from Wadás model is almost a linear function of mole fraction and can be considered as temperature independent for a fixed mole fraction over the whole composition range. The results were analysed and discussed from the structural changes point of view in aqueous medium.

1. Introduction

Due to their very low vapour pressures, the contribution of ILs for air pollution is negligible. However, ILs may have a significant solubility in water. Therefore, they may contaminate water streams, leading to environmental problems. Due to their structure and ionic interactions, ionic liquids and their mixtures with molecular species exhibit unique properties. Strong ion-ion interactions present in ionic liquids lead to highly organised three-dimensional supramolecular polymer networks of cations and anions joined by hydrogen bonds and/or Coulomb interactions, where the force of ion–ion interaction depends on the ionic liquid structure, and can greatly affect the ability of the anions or cations to interact with dissolved species [1].

Some ILs are considerably hydrophilic and their aqueous solutions have become the subject of a considerable amount of work exploring aqueous solutions of ILs as great potential for a wide range of applications in different areas, such as extraction processes [2], aqueous biphasic systems [3], and organic and inorganic synthetic reactions [4]. Nonetheless, the success of designing and/or developing a process based on these systems relies on the knowledge and accurate characterisation of their thermophysical properties.

PILs were produced by a stoichiometric acid\base Brønsted reaction and their main difference, compared to aprotic ILs (AILs), is the presence of at least a proton, which is/are able to promote extensive hydrogen bonding [5]. These liquids present some characteristics, such as a slightly lower conductivity and stability,

* Corresponding author. Tel.: +351 239 798 729; fax: +351 239 798 703.
E-mail addresses: abel@eq.uc.pt, fabel7@gmail.com (A.G.M. Ferreira).

http://dx.doi.org/10.1016/j.jct.2016.01.028
0021-9614/

which may reduce, at first, their interest for a number of applications. However, their low cost, simple synthesis and purification methods, low toxicity and high biodegradation character, among other aspects of appealing characteristics, overcome those limitations for many different purposes. The ionic liquids from substituted hydroxyethylammonium cations and organic acid anions can be obtained by simple synthesis [6,7], and have important applications [8]. Moreover, it was verified that some ILs of that family present a negligible toxicity [9].

Among several thermodynamic properties, the volumetric and acoustical properties are very important for the design of an industrial process as for theoretical studies. For instance, the knowledge of the excess molar volume, isentropic compressibility, and apparent molar properties is essential to develop reliable predictive models [10,11], as well as to understand the nature of solute–solvent and solute–solute interactions.

Studies covering aqueous solutions of ILs properties are, typically, divided into three approaches: the description of the dilute region of the aqueous solutions of ILs, the investigation of the water content effect on the pure ILs properties, and the characterisation over the entire composition range. In our previous paper [12], detailed literature information is provided for each approach.

The density and speed of sound measurements for hydroxyethylammonium (HEA) cation based ILs with organic acid anions and mixed with solvents are scarce. Iglesias *et al.* [7] reported densities and speed of sound for mixtures of 2-hydroxyethylammonium formate with short hydroxylic solvents (water, methanol and ethanol) while Álvarez *et al.* [13] for mixtures of 2-hydroxyethylammonium acetate with the same solvents. The density of hydroxyethylammonium cation-based ILs with organic acid anions has been reported by Kurnia *et al.* [14–16], for mixtures composed of 2-hydroxyethylammonium formate, acetate, propionate, and lactate with methanol [14] and bis(2-hydroxyethyl)methylammonium formate and acetate with alcohols [15,16], and by Taib and Murugesan [17] for aqueous mixtures of bis(2-hydroxyethyl)ammonium acetate.

As a continuation of the previous research by the authors [12], this work aims to measure the speed of sound in pure m2HEAB and m2HEAP at temperatures ranging from (293.15 to 343.15) K and the speed of sound and density of their aqueous solutions over the entire concentrations range for temperatures from (298.15 to 333.15) K, at atmospheric pressure. The results were used to obtain important derived properties, such as the IL apparent molar volume (V_ϕ) and compressibility (k_ϕ), excess molar volume (V_m^E) and isentropic compressibility (k_S). All these properties were successfully represented by analytical functions over the entire concentration and temperature ranges of the measurements. The apparent molar volume of the aqueous solutions of ILs was represented by the Pitzer–Simonson equations [18]. This equation has been used to describe the volumetric behaviour of aqueous ionic liquids in all the IL concentration range, thus overcoming the limitations of models based on Debye-Hückel theory applicable to very dilute solutions of salts. The evaluated apparent molar properties were used to study the effect of the IL–water and IL–IL interactions.

2. Experimental

Water (mili-Q) was used for preparation of the aqueous solutions. The N-methyl-2-hydroxyethylammonium butyrate and N-methyl-2-hydroxyethylammonium pentanoate were prepared from stoichiometric quantities of the 2-methylaminoethanol with butanoic and pentanoic acids using the methodology described in detail by Talavera-Prieto *et al.* [8]. The IL water content was determined with a Metrohm 831 Karl Fisher coulometer indicating a water mass fraction lower than $3{\cdot}10^{-4}$. The mixtures (IL + water) were prepared by mass using a Mettler AT 200 balance with an uncertainty of $\pm10^{-5}$ g. The uncertainty in the mole fraction was estimated as being of $\pm10^{-4}$. Table 1 summarises relevant information on compounds purities, water content and suppliers.

The densities were measured using an Anton Paar DMA 60 digital vibrating tube densimeter, with a DMA 512P measuring cell. The measuring setup and the vibrating tube densimeter calibration were described in detail in our work [19]. The expected uncertainty for the density, due to viscosity of the ionic liquid and its aqueous solutions (damping effects on the vibrating tube), was determined to be, within the temperature range adopted, 0.3 $kg{\cdot}m^{-3}$ maximum [19]. The uncertainties in temperature, T, and pressure, p, were determined to be $u(T) = \pm0.02$ K and $u(p) = \pm0.03$ MPa, respectively. The combined standard uncertainty of the density measurements, ρ, estimated taking into account the influence of uncertainties associated with the calibration equation [19], temperature, pressure, period of oscillations (six-digit frequency counter), viscosity, and calibrating fluids density data, was $u(\rho) = \pm0.86$ $kg{\cdot}m^{-3}$.

A stainless steel cell was designed for the speed of sound measurement. Two 5 MHz ultrasonic transducers (one acting as a transmitter and the other as a receiver) were mounted in cavities drilled on its plane surfaces. The ultrasound wave propagation time corresponding to the path between the transmitter and receiver was collected and displayed by an oscilloscope, and then transferred to a computer for processing. The time of flight in the mixture, $\triangle\tau$, was obtained subtracting the time that the acoustical wave takes to travel between the emitter and receiver from the propagation time in the cell steel walls. The cell was calibrated by measuring $\triangle\tau$ in water, toluene, and 1,2-butanediol at atmospheric pressure. The measuring setup and the cell calibration were described with detail in a previous publication [20] where the speed of sound combined standard uncertainty was determined to be $u(u) = \pm1.2$ $m{\cdot}s^{-1}$.

The density and speed of sound measurements of the binary mixtures were made with the DMA 512P and the acoustical cells open to the atmosphere. The measurement of the atmospheric pressure was made using a calibrated pressure transducer (AFRISO Euro-Index, DMU03). Taking the observed values covering February and March the mean value was $p = (102.24 \pm 0.39)$ kPa.

TABLE 1
Purities of the synthesis materials and ionic liquids.

Chemical	Supplier (CAS N)	Mass fraction purity	Water content
2-Methylaminoethanol[a]	Sigma-Aldrich (109-83-1)	0.99	<0.005
Butanoic acid[a]	Sigma-Aldrich (107-92-6)	>0.995	<0.005
Pentanoic acid[a]	Sigma-Aldrich (109-52-4)	>0.995	<0.005
m2HEAB[b]		>0.99	$3{\cdot}10^{-4}$
m2HEAP[b]		>0.99	$3{\cdot}10^{-4}$

[a] These materials were used as received, as the water content could be removed after the synthesis.
[b] The ILs were fully distiled under high vacuum (10^{-4} Pa) and the distillate purity checked by ^{1}H NMR and ^{13}C NMR [21]. The final water content was determined with a Metrohm 831 Karl Fisher coulometer.

3. Results and discussion

3.1. Properties of pure substances

The experimental values for the density and speed of sound of m2HEAB and m2HEAP at atmospheric pressure and temperatures range, T = (293.15 to 343.15) K, together with the molar volume, V_m, and the isentropic compressibility, k_S, are presented in table 2.

The isentropic compressibility can be defined using the equation:

$$k_S = -\frac{1}{V_m}\left(\frac{\partial V_m}{\partial p}\right)_S = \frac{1}{\rho}\left(\frac{\partial \rho}{\partial p}\right)_S = \left(\frac{\partial \ln \rho}{\partial p}\right)_S, \quad (1)$$

where S is the entropy. The isentropic compressibility is determined from the sound velocity using the Laplace–Newtońs equation:

$$k_S = \frac{1}{\rho u^2}. \quad (2)$$

The densities of m2HEAB and m2HEAP were taken from a previous work [8]. For these substances the density and the molar volume behave as expected, *i.e.*, the density decreases and the molar volume increases as temperature increases. Concerning the speed of sound, it decreases with the temperature increase leading thus, to the isentropic compressibility increase. In table 2, the isobaric molar heat capacity $C_{p,m}$, determined using the empirical equations reported in our previous publication [8], is also reported.

The thermal expansivity, α_p, of pure substances, required to calculate the excess properties of the m2HEAB and m2HEAP aqueous mixtures, can be determined using the equation:

$$\alpha_p = \frac{1}{V_m}\left(\frac{\partial V_m}{\partial T}\right)_p = -\frac{1}{\rho}\left(\frac{\partial \rho}{\partial T}\right)_p = -\left(\frac{\partial \ln \rho}{\partial T}\right)_p. \quad (3)$$

The polynomial functions

$$\ln(\rho/\mathrm{kg\cdot m^{-3}}) = 7.1276 - 5.9229\cdot 10^{-4}(T/K) - 9.65401\cdot 10^{-8}(T/K)^2 \quad (4)$$

and

$$\ln(\rho/\mathrm{kg\cdot m^{-3}}) = 7.1205 - 7.1229\cdot 10^{-4}(T/K) - 9.9988\cdot 10^{-8}(T/K)^2, \quad (5)$$

were found adequate to correlate the density variation with temperature, at atmospheric pressure, of the m2HEAB and m2HEAP ILs, with standard deviations less than 10^{-5} kg·m^{-3}. From equations (4) and (5) combined with equation (3), the thermal expansivity of the ionic liquid was calculated for the temperature values given in table 2. The thermal expansivity values agree within 2.8% with the ones derived from density measurements reported by Alvarez *et al.* [21].

3.2. Volumetric properties of liquid mixtures

The densities of pure m2HEAB and m2HEAP, at atmospheric pressure, were taken from a previous publication [8] where density was determined for the (298.15 to 358.15) K temperature range and (0.1 to 25) MPa pressure range. The density of the aqueous mixtures of the studied ILs were determined for temperatures ranging from (298.15 to 333.15) K covering all the mole fraction range and are presented in table 3.

The experimental density of the ILs mixtures were correlated using the rational function,

$$\ln \rho = x_1 \ln \rho_1 + x_2 \ln \rho_2 + x_1 x_2 \frac{\sum_{i=0}^{m}(C_{i0} + C_{i1}T)(2x_1 - 1)^i}{1 + \sum_{j=1}^{n}(D_{j0} + D_{j1}T)(2x_1 - 1)^j}, \quad (6)$$

where C_{ik} (k = 0, 1) and D_{jk} (k = 0, 1) are adjustable coefficients obtained by fitting equation (6) to the variations of $\Delta \ln \rho / x_1 x_2$ (= $(\ln \rho - x_1 \ln \rho_1 - x_2 \ln \rho_2)/x_1 x_2$) using simultaneously the investigated temperatures and compositions. Those variations evidence the characteristic hyperbolic shape with a steep increase near x_1 = 0 (see figure S1). This behaviour supports the use of the rational functions to represent effectively the anomalous dependences of

TABLE 2
Density, ρ, molar volume V_m, speed of sound u, isentropic compressibility k_S, isobaric molar heat capacity $C_{p,m}$, and thermal expansivity α_p of m2HEAB and m2HEAP at temperatures between (293.15 and 343.15) K and p = 0.102 MPa.[a]

T/K	ρ/(kg·m^{-3})[b]	V_m/(cm^3·mol^{-1})	u/(m·s^{-1})	$10^{10}\kappa_s$/(Pa^{-1})	$C_{p,m}$/(J·K^{-1}·mol^{-1})[d]	$10^4\,\alpha_p$/(K^{-1})
			m2HEAB			
293.15	1038.7[c]	157.140	1576.8	3.872	359.40	6.489
298.15	1035.3	157.651	1562.9	3.954	361.92	6.499
303.15	1031.9[c]	158.165	1548.0	4.044	364.44	6.508
308.15	1028.6	158.681	1529.7	4.155	366.96	6.518
313.15	1025.2[c]	159.199	1511.9	4.267	369.47	6.528
318.15	1021.9	159.720	1499.4	4.353	371.99	6.537
323.15	1018.5[c]	160.243	1481.3	4.474	374.51	6.547
328.15	1015.2	160.769	1467.2	4.576	377.03	6.556
333.15	1011.9[c]	161.297	1451.2	4.693	379.55	6.566
338.15	1008.6	161.828	1436.7	4.803	382.07	6.576
343.15	1005.3[c]	162.362	1419.4	4.937	384.58	6.585
			m2HEAP			
293.15	1012.6[c]	175.031	1537.0	4.180	398.20	6.537
298.15	1009.3	175.603	1516.3	4.309	400.00	6.527
303.15	1006.0[c]	176.177	1503.7	4.396	401.81	6.517
308.15	1002.8	176.751	1486.5	4.513	403.61	6.507
313.15	999.6[c]	177.327	1471.0	4.624	405.41	6.497
318.15	996.3	177.903	1457.0	4.728	407.22	6.487
323.15	993.1[c]	178.481	1440.0	4.856	409.02	6.477
328.15	989.9	179.041	1424.6	4.977	410.82	6.467
333.15	986.7[c]	179.639	1412.8	5.078	412.63	6.457
338.15	983.5	180.219	1397.1	5.209	414.43	6.447
343.15	980.3[c]	180.801	1381.9	5.342	416.23	6.437

[a] Standard uncertainties u are: $u(T)$ = ±0.02 K, $u(p)$ < ±0.03 MPa, $u(\rho)$ = ±0.86 kg·m^{-3}, $u(u)$ = ±1.2 m·s^{-1}.
[b] Experimental data by Talavera-Prieto *et al.* [8].
[c] Extrapolated values from equations (4) and (5) for m2HEAB and m2HEAP, respectively.
[d] From $C_{p,m}$/(J·K^{-1}·mol^{-1}) = 211.74 + 0.5037 (T/K) and $C_{p,m}$/(J·K^{-1}·mol^{-1}) = 292.46 + 0.3607 (T/K) for m2HEAB and 2mHEAP, respectively [8].

TABLE 3
Experimental density, ρ and speed of sound u, as a function of the composition, expressed as mole fraction of ionic liquid, x_1, and molality, m_{IL}, for the aqueous solutions of ionic liquids m2HEAB and m2HEAP at temperatures between (298.15 and 333.15) K and p = 0.102 MPa.[a]

x_1	m_{IL}/(mol·kg^{-1})	ρ/(kg·m^{-3})	u/(m·s^{-1})	ρ/(kg·m^{-3})	u/(m·s^{-1})	ρ/(kg·m^{-3})	u/(m·s^{-1})	ρ/(kg·m^{-3})	u/(m·s^{-1})
					m2HEAB				
		T = 298.15 K		*T* = 303.15 K		*T* = 308.15 K		*T* = 313.15 K	
0.0000	0.00	997.1[c]	1496.7[c]	995.7[c]	1509.2[c]	994.0[c]	1519.8[c]	992.2[c]	1528.9[c]
0.0199	1.13	1016.9	1645.6	1013.1	1646.1	1009.2	1646.7	1005.3	1647.3
0.0497	2.90	1035.0	1762.6	1032.4	1755.1	1029.8	1747.6	1027.2	1740.0
0.1005	6.20	1040.8	1773.4	1037.9	1763.6	1035.0	1753.8	1032.0	1744.0
0.1960	13.5	1050.5	1739.5	1047.4	1725.4	1044.4	1711.3	1041.3	1697.2
0.3008	23.9	1052.5	1732.0	1049.4	1717.0	1046.3	1701.9	1043.2	1686.8
0.4005	37.1	1049.1	1693.9	1046.0	1678.1	1042.8	1662.3	1039.6	1646.5
0.5090	57.5	1046.8	1674.1	1043.6	1658.3	1040.4	1642.4	1037.2	1626.6
0.5968	82.2	1045.0	1659.6	1041.7	1643.9	1038.5	1628.1	1035.3	1612.4
0.8069	232.0	1041.3	1630.4	1038.0	1614.5	1034.7	1598.6	1031.4	1582.7
1.0000		1035.3[b]	1562.9	1031.9[b]	1548.0	1028.6[b]	1529.7	1025.2[b]	1511.9
		T = 318.15 K		*T* = 323.15 K		*T* = 328.15 K		*T* = 333.15 K	
0.0000	0.00	990.2[c]	1536.4[c]	988.0[c]	1542.6[c]	985.7[c]	1547.4[c]	983.2[c]	1551.0[c]
0.0199	1.13	1001.5	1647.8	997.6	1648.4	993.7	1648.9	989.9	1649.5
0.0497	2.90	1024.6	1732.5	1022.0	1725.0	1019.4	1717.5	1016.8	1709.9
0.1005	6.20	1029.1	1734.2	1026.2	1724.5	1023.2	1714.7	1020.3	1704.9
0.1960	13.5	1038.3	1683.1	1035.2	1669.0	1032.2	1654.9	1029.1	1640.8
0.3008	23.9	1040.1	1671.7	1036.9	1656.6	1033.8	1641.6	1030.7	1626.5
0.4005	37.1	1036.4	1630.6	1033.3	1614.8	1030.1	1599.0	1026.9	1583.1
0.5090	57.5	1034.0	1610.7	1030.9	1594.8	1027.7	1579.0	1024.5	1563.1
0.5968	82.2	1032.1	1596.6	1028.9	1580.8	1025.6	1565.1	1022.4	1549.3
0.8069	232.0	1028.1	1566.8	1024.9	1550.9	1021.6	1535.0	1018.3	1519.1
1.0000		1021.9[b]	1499.4	1018.5[b]	1481.3	1015.2[b]	1467.2	1011.9[b]	1451.2
					m2HEAP				
		T = 298.15 K		*T* = 303.15 K		*T* = 308.15 K		*T* = 313.15 K	
0.0000	0.00	997.1[c]	1496.7[c]	995.7[c]	1509.2[c]	994.0[c]	1519.8[c]	992.2[c]	1528.9[c]
0.0199	1.13	1013.0	1645.3	1009.6	1644.5	1006.1	1643.7	1002.7	1642.9
0.0500	2.92	1026.0	1705.8	1022.7	1698.6	1019.3	1691.5	1015.9	1684.3
0.0988	6.09	1027.5	1670.2	1024.2	1659.8	1020.9	1649.5	1017.7	1639.1
0.2023	14.1	1029.9	1644.9	1026.8	1631.5	1023.7	1618.1	1020.7	1604.8
0.3000	23.8	1028.5	1633.5	1025.4	1618.8	1022.3	1604.2	1019.2	1589.6
0.4053	37.8	1025.2	1609.2	1022.1	1594.7	1018.9	1580.2	1015.8	1565.7
0.5003	55.6	1021.0	1583.7	1017.8	1568.6	1014.6	1553.5	1011.5	1538.4
0.5993	83.0	1019.1	1571.3	1015.9	1556.3	1012.7	1541.4	1009.5	1526.5
0.8061	230.8	1013.3	1541.8	1010.1	1526.5	1006.9	1511.2	1003.6	1495.9
1.0000		1009.3[b]	1516.3	1006.0[b]	1503.7	1002.8[b]	1486.5	999.6[b]	1471.0
		T = 318.15 K		*T* = 323.15 K		*T* = 328.15 K		*T* = 333.15 K	
0.0000	0.00	990.2[c]	1536.4[c]	988.0[c]	1542.6[c]	985.7[c]	1547.4[c]	983.2[c]	1551.0[c]
0.0199	1.13	999.3	1642.2	995.8	1641.4	992.4	1640.6	988.9	1639.8
0.0500	2.92	1012.6	1677.2	1009.2	1670.0	1005.9	1662.8	1002.5	1655.7
0.0988	6.09	1014.4	1628.8	1011.1	1618.5	1007.8	1608.1	1004.5	1597.8
0.2023	14.1	1017.6	1591.4	1014.6	1578.0	1011.5	1564.6	1008.5	1551.2
0.3000	23.8	1016.1	1575.0	1012.9	1560.4	1009.8	1545.7	1006.7	1531.1
0.4053	37.8	1012.7	1551.2	1009.5	1536.7	1006.4	1522.2	1003.2	1507.7
0.5003	55.6	1008.3	1523.3	1005.1	1508.2	1002.0	1493.1	998.8	1478.1
0.5993	83.0	1006.3	1511.5	1003.1	1496.6	999.9	1481.7	996.7	1466.7
0.8061	230.8	1000.4	1480.6	997.2	1465.3	993.9	1450.0	990.7	1434.6
1.0000		996.3[b]	1457.0	993.1[b]	1440.0	989.9[b]	1424.6	986.7[b]	1412.8

[a] Standard uncertainties u are: $u(T)$ = ±0.02 K, $u(p)$ = ±0.39 kPa (for aqueous mixtures of ILs), $u(p)$ < ±0.03 MPa (for pure ionic liquids), $u(x_{IL})$ = ±10^{-4}, $u(m)$ = ±0.002 mol·kg^{-1}, $u(\rho)$ = ±2 kg·m^{-3} (max), $u(u)$ = ±7 m·s^{-1} (max).
[b] Experimental values by Talavera-Prieto *et al.* [8].
[c] From NIST: http://webbook.nist.gov/chemistry/fluid/ (accessed July 2014).

the thermodynamic properties with the composition [22]. The parameters C_{ik} and D_{jk} of equation (6) are presented in table 4. The description of the density using these equations, with only 10 and 12 coefficients, is good for the whole temperature and composition ranges, with standard deviations close to the experimental standard uncertainty of the measurements. The percentage relative deviations between the calculated density values, obtained by equation (6), and the experimental ones are lower than 0.2%, as depicted in figure 1, meaning less than ±2 kg·m^{-3}. However, some density scatter is observed for fixed composition at some temperatures. The scatter at low ionic liquid content (x_1 < 0.1) must be due to the strong change in density with composition: in this range, errors of ±0.001 in the mole fraction could give uncertainties about ±2 kg·m^{-3}. Beyond this range, the errors in the composition will be certainly of minor influence in density uncertainty (possibly less than ±1 kg·m^{-3}). It is possible that real uncertainty in the mole fraction could be sometimes greater than the given standard uncertainty (±10^{-4}) and thus the uncertainty in density could reach at the worst situation a maximum of ±2 kg·m^{-3}. We made the analysis of ($\rho_{eq.(6)} - \rho_{exp}$) deviations for (m2HEAB + H_2O) mixtures and we have found that 63% of the measurements show deviations within one standard deviation (±1 kg·m^{-3}) as almost expected statistically for random errors occurring in the measurements. Therefore the maximum uncertainty for the measurement of density of the aqueous IL mixtures will be at worst situation ±2 kg·m^{-3}.

For the binary systems, the excess molar volumes, V^E_m, were calculated using the experimental mixture and the pure compounds densities, as described by equation (7):

TABLE 4
Fitting parameters C_{ik}, C_{jk}, average absolute deviation *AAD*%, and standard deviation σ, for density and speed of sound of binary aqueous systems by equations (6) and (18) respectively.

Mixture	m2HEAB(1) + H_2O(2)		m2HEAP(1) + H_2O(2)	
Parameter	ln ρ/(kg·m^{-3})	u/(m·s^{-1})	ln ρ/(kg·m^{-3})	u/(m·s^{-1})
C_{00}	0.23360	3565.65	$-5.5220\cdot10^{-2}$	3036.70
C_{01}	$-3.6717\cdot10^{-4}$	−9.95364	$5.4262\cdot10^{-4}$	−9.10821
C_{10}	0.23764	2053.99	1000.63	2650.35
C_{11}	$-3.67711\cdot10^{-4}$	−5.60217	−5.22389	−8.2298
C_{20}	$4.1823\cdot10^{-3}$	−891.275	−503.888	−533.01
C_{21}	$-5.9104\cdot10^{-5}$	3.97366	1.91384	1.48736
C_{30}	0	0	−1874.58	0
C_{31}	0	0	7.05064	0
D_{10}	1.79096	3.43479	27891.3	3.38372
D_{11}	$6.7754\cdot10^{-4}$	$-6.9964\cdot10^{-3}$	−117.194	$-5.0522\cdot10^{-3}$
D_{20}	0.80111	2.30968	27595.3	2.47402
D_{21}	$5.8872\cdot10^{-4}$	$-6.4942\cdot10^{-3}$	−116.102	$-5.3745\cdot10^{-3}$
AAD%	0.08	0.31	0.05	0.16
σ_ρ (*or* σ_u)	0.95	7.3	0.69	3.3

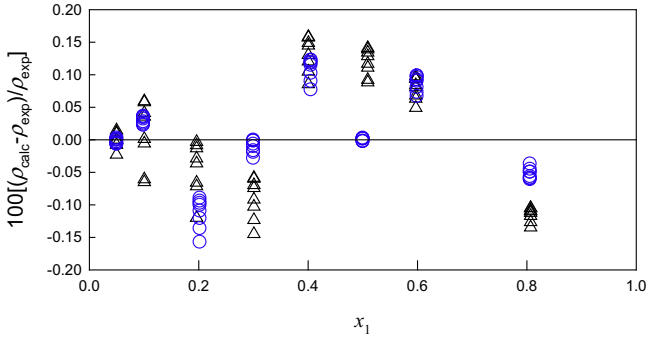

FIGURE 1. Relative deviations between the calculated density, (ρ_{calc}) with correlation equation (6) and the experimental values (ρ_{exp}) for the aqueous mixtures of ILs as function of IL mole fraction x_1 and temperature: Δ, {m2HEAB(1) + H_2O(2)}; ○, {m2HEAP(1) + H_2O(2)}.

$$V_m^E = \frac{M}{\rho} - \frac{x_1 M_1}{\rho_1} - \frac{x_2 M_2}{\rho_2}, \tag{7}$$

where ρ is the density of the mixture and $M = (x_1M_1 + x_2M_2)$ is the corresponding molar mass.

Using the experimental density and the mole fraction uncertainties, the uncertainty in V_m^E, $u(V_m^E)$, is estimated, using the errors propagation method, to be ±0.10 cm^3·mol^{-1} at the upper limit of ionic liquid concentrations and ±0.03 cm^3·mol^{-1} at the lower limit.

The binary V_m^E experimental values were fitted by means of Redlich–Kister polynomials:

$$V_m^E/(\mathrm{cm}^3\cdot\mathrm{mol}^{-1}) = x_1x_2\sum_{i=0}^{2}(A_{i,0} + A_{i,1}T)(2x_1 - 1)^i, \tag{8}$$

where A_{ij} ($j = 0, 1$) are adjustable coefficients given in table 5 together with the standard deviation $\sigma(V_m^E)$. The experimental values of the excess molar volumes for the binary systems are plotted in figure 2. The V_m^E values take negative values at all temperatures and over the entire composition range. Furthermore, its temperature dependency is very small, while for fixed compositions and ionic liquid mole fractions ranging between 0.2 and 0.6 are significantly negative (less than −1 cm^3·mol^{-1}).

It is observed that the V_m^E curves are asymmetric with a minimum at mole fractions of ionic liquid between 0.3 and 0.4. A similar behaviour was found for the {m2HEAPr(1) + H_2O(2)} system studied by the authors [12]. The significant magnitude and negative sign of the V_m^E values reflect the type of interactions taking place between the species, which are the result of different effects, namely the breakdown of the self-associated water molecules (positive contribution to volume), the packing effect, and the ion–dipole interaction of water molecules with ionic liquid (negative contributions to the volume). The minimum of the V_m^E at IL mole fractions ranging from 0.3 to 0.4 corresponds to the highest packing between water and ionic liquid. The molar volumes of the pure ILs are higher than 150 cm^3·mol^{-1} in all the temperature range, being much greater than the molar volume of water (18.02 cm^3·mol^{-1}). These large differences between molar volumes have as a consequence that the small water molecules will occupy the available space or free volume of the ionic liquid upon mixing. From the molecular dynamics (MD) studies by Bernardes *et al.* [23], an approximate picture of the structure of N-methyl-2-hydroxyethylammonium (ILs + water) mixtures within the composition range where the V_m^E minimum occurs can be made. The introduction of water into the polar network will be responsible by increase in the cation–cation and anion–anion distance due to the ability of water to interact with (and partially destroy) the polar network. In the evaluated composition range, the authors identified intermeshed types of chain-like networks with different degrees of aggregation: (i) the IL polar network, that is stretched but still continuous at lower water content becoming more fragmented as water increase; (ii) at moderate water mole fractions there will be a water network composed by chains of water molecules, with very little branching; and (iii) a water–anion network possibly formed by alternating anions and water molecules, could exist at intermediate/high water mole fractions of 0.7 to 0.8. Anyway, ionic liquid pairs can form at very dilute IL aqueous mixtures. Applying X-ray scattering techniques to (2-hydroxyethylammonium + water) solutions, Alvarez *et al.* report the formation of pairs from ionic liquid at IL mole fraction near 0.08 [13].

The apparent molar volumes, V_ϕ, of the PILs in the aqueous mixtures were calculated using equation (9):

$$V_\phi = \frac{M_1}{\rho} + \frac{(\rho_2 - \rho)}{m\rho_2\rho}, \tag{9}$$

where m (mol·kg^{-1}) is the molality of IL in water. From the error in mole fraction the maximum uncertainty in molality, $u(m)$, is estimated to be ±0.002 mol·kg^{-1}. The uncertainty in V_ϕ, $u(V_\phi)$, was obtained from the errors propagation method and is on the order of ±0.57 cm^3·mol^{-1} for the low ionic liquid content region, decreasing to ±0.11 cm^3·mol^{-1} for higher IL concentrations. The calculated apparent molar volumes are given in table S1 as supplementary

TABLE 5
Fitting parameters of equation (8) used for analytical representation of V^E_m, and of equation (20) used for $k_S{}^E$, and u^E with 95% of confidence limits for the {m2HEAB(1) + H_2O(2)} and {m2HEAP(1) + H_2O(2)} systems.

	A_{0k}	A_{1k}	A_{2k}	B_{1k}	B_{2k}	
			$V^E_m/(cm^3{\cdot}mol^{-1})$			
			m2HEAB			
$k=0$	−3.06061	4.50264	−6.03123			$\sigma(V^E_m)=0.068$
$k=1$	$-7.2674{\cdot}10^{-3}$	$-9.1059{\cdot}10^{-3}$	$6.9325{\cdot}10^{-3}$			
			m2HEAP			
$k=0$	−3.42737	5.18485	−14.1482			$\sigma(V^E_m)=0.060$
$k=1$	$-5.3816{\cdot}10^{-3}$	$-7.8097{\cdot}10^{-3}$	$3.9243{\cdot}10^{-2}$			
			$10^{10}/k^E_S(Pa^{-1})$			
			m2HEAB			
$k=0$	−6.75267	−20.1372	1.25162	6.8384	5.4219	$\sigma(k_S{}^E)=0.038$
$k=1$	$1.0954{\cdot}10^{-2}$	$5.8129{\cdot}10^{-2}$	$-1.0006{\cdot}10^{-2}$	$-1.8066{\cdot}10^{-2}$	$-1.6556{\cdot}10^{-2}$	
			m2HEAP			
$k=0$	−7.00032	−1.28769	−1.85397	1.03282	0	$\sigma(k_S{}^E)=0.039$
$k=1$	$1.4212{\cdot}10^{-2}$	$4.2158{\cdot}10^{-3}$	$5.6650{\cdot}10^{-3}$	$-1.9205{\cdot}10^{-4}$	0	
			$u^E/(m{\cdot}s^{-1})$			
			m2HEAB			
$k=0$	2192.912	249.9751	407.5004	0.98182	0	$\sigma(u^E)=8.8$
$k=1$	−5.13791	−0.31384	$6.9122{\cdot}10^{-2}$	$-1.8217{\cdot}10^{-4}$	0	
			m2HEAP			
$k=0$	1829.375	187.2036	163.0799	0.94655	0	$\sigma(u^E)=8.5$
$k=1$	−4.61251	−0.66194	−0.27260	$9.1520{\cdot}10^{-5}$	0	

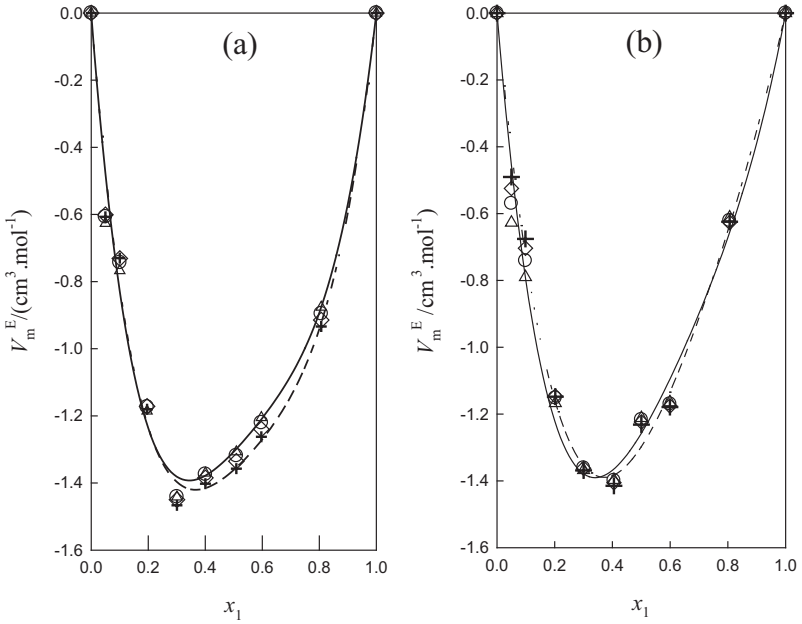

FIGURE 2. Excess molar volumes, V^E_m, as a function of ammonium IL mole fraction, x_1 at temperatures of 298.15 K (Δ), 308.15 K (○), 318.15 K (◇), 328.15 K (+), for {m2HEAB (1) + H_2O(2)} (a), and {m2HEAP(1) + H_2O(2)} (b). Solid and dashed curves were calculated from equation (8) at T = (298.15 and 328.15) K, respectively.

information and plotted in figure 3 as function of the IL molality and temperature.

The apparent molar volume increases rapidly at low concentrations (up to $m \approx 25$ kg·mol^{-1}) and then it is almost constant.

The apparent molar volumes as function of IL molality and temperature, for the whole concentration and temperature ranges, were described by the following equation:

$$V_\phi = V^0_\phi(T) + \frac{A_V(T)(m)^{1/2} + B_V(T)m}{1 + C_V(T)m}, \qquad (10)$$

where $V^0_\phi(T)$, $A_V(T)$, $B_V(T)$, and $C_V(T)$ are functions of temperature: $V^0_\phi = v_0 + v_1T + v_2T^2$, $A_V(T) = a_0 + a_1T$, $B_V(T) = b_0 + b_1T + b_2T^2$, $C_V(T) = c_0 + c_1T$. The quadratic terms in temperature are needed in order for the equation to be able to describe the small curvature on the temperature observed for low IL concentrations (see figure 4).

For the dilute solution of IL ($m \to 0$) equation (10) gives the empirical Redlich–Rosenfeld–Meyer equation [24]:

$$V_\phi = V^0_\phi + A_V(m)^{1/2} + B_V m, \qquad (11)$$

derived from the Debye-Hückel limiting law. In equations (10) and (11) V^0_ϕ is the apparent molar volume at infinite dilution (equal to the partial molar volume at infinite dilution). The parameters v_i, a_i, b_i and c_i of equation (10) are reported in table 6. The correlation of apparent molar volume with equation (10) is excellent as depicted in figure 3 where equation (10) is plotted as solid lines. The standard deviations of fittings are small of 0.25 cm^3·mol^{-1} and 0.24 cm^3·mol^{-1} respectively for the aqueous mixtures of m2HEAB and m2HEAP.

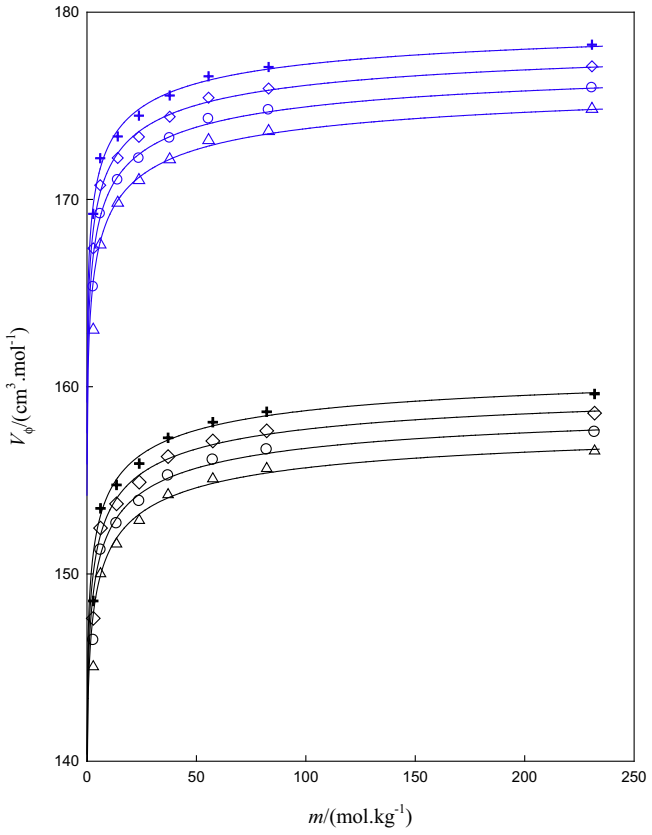

FIGURE 3. Apparent molar volume, V_ϕ, versus molality, m, at several temperatures for {2mHEAB(1) + H_2O(2)} (black) and {m2HEAP(1) + H_2O(2)} (blue): Δ, 298.15 K; ○, 308.15 K; ◇, 318.15 K; +, 328.15 K. Solid curves were calculated from equation (10). (For interpretation of the references to colour in this figure legend, the reader is referred to the web version of this article.)

3.2.1. Pitzer–Simonson equation

The thermodynamics of electrolyte solutions have been successfully developed using a semi-empirical model based upon a virial series in molality and an extended Debye–Huckel term [25,26]. However the model fails at very high concentrations of salt, as the molality becomes infinite for the pure salt. An alternative mole-fraction-based model has been developed by Pitzer and Simonson [18] for electrolytes of symmetrical charge type. In that model, the excess Gibbs energy, G^E, is given by the sum of a term for short-range interactions (Margules type) and a Debye–Huckel term [27]. Given a symmetrical charged ionic liquid MX as the solute, dissociated in M and X ions, the mole fraction of the solvent can be expressed as $x_s = n_S/(n_S + 2n_{MX})$ and the mole fraction of the solute is $x_M = x_X = n_{MX}/(n_S + 2n_{MX})$ where n is the number of moles of the species. The ionic mole fraction is defined as $x_I = (n_M + n_X)/(n_S + n_M + n_X)$ and therefore $x_I = x_M + x_X = 1 - x_S$. For a MX symmetrical charged ionic liquid, the ionic mole fraction is [28] $x_I = 2m/(2m + m_S)$ where m_s ($m_s = 1/M_s$) is the molality of solvent with molar mass M_s ($m_s = 55.5084$ mol·kg^{-1} for water). From the excess Gibbs energy the equations for apparent molar volume can be derived. One equation is [27]:

$$V_\phi = \overline{V_\phi^0} - 2RTx_I\left[W^V_{s,MX} - x_s U^V_{s,MX}\right] + \left(\frac{A^V_x}{b}\right)\ln(1 + bI_x^{1/2}), \quad (12)$$

where $\overline{V_\phi^0}$ is the partial molar volume of the ionic liquid at infinite dilution (taken also as V_ϕ^0), I_x is the ionic strength for MX on a mole fraction basis calculated as [27]:

$$I_x = (1/2)\sum x_i z_i^2 = x_M = x_X = (1 - x_s)/2, \quad (13)$$

where z_i is the charge of the ith ion. The parameter $b = 2150(\rho_s/\varepsilon T)^{1/2}$ is related to a hard-core collision diameter [29] (ρ_s is the density of solvent and ε the dielectric constant). The parameters $W^V_{s,MX}$ and $U^V_{s,MX}$ in equation (12) characterising the short-range part of G^E, are both functions of temperature and pressure, and specific to each solute. The Debye–Huckel parameters are:

$$A^V_x = m_s^{1/2}A^V, \quad A^V = -4RT\left(\frac{\partial A\phi}{\partial P}\right)_T, \quad (14)$$

where the A^V values are the Debye–Hückel limiting slope mentioned before, reflecting the volumetric and dielectric properties of solvent and were tabulated at different temperatures by Archer and Wang [30]. Equation (12) can be also written as:

$$Y = V_\phi - \left(\frac{A^V_x}{b}\right)\ln(1 + bI_x^{1/2}) = \bar{V}^0_\phi + 2RTx_I\left[U^V_{s,MX} - W^V_{s,MX}\right] - 2RTx_I^2 U^V_{s,MX}. \quad (15)$$

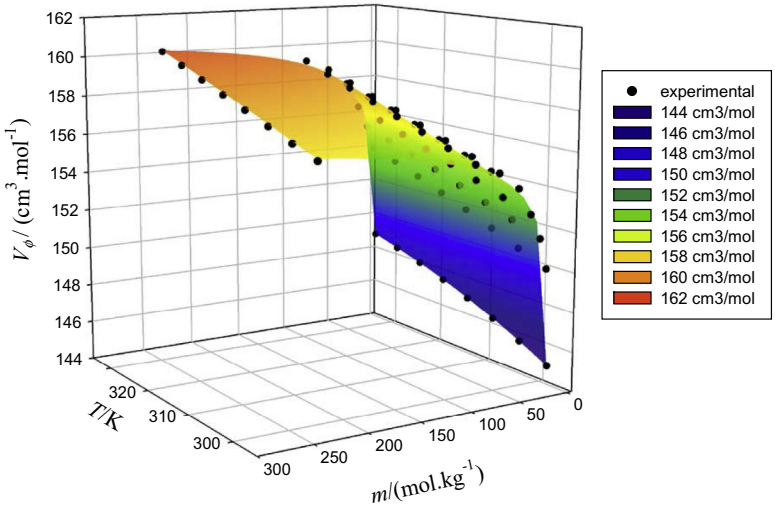

FIGURE 4. Apparent molar volume *versus* molality and temperature for aqueous solutions of m2HEAB. The coloured surface represents the fitted equation (10) to data.

TABLE 6
Fitting parameters, and standard deviation σ, for apparent molar volume and apparent molar isentropic compressibility of binary IL aqueous systems by equations (10) and (24) respectively.

Mixture	m2HEAB(1) + H_2O(2)		m2HEAP(1) + H_2O(2)	
Parameter	V_ϕ/(cm^3·mol^{-1})	k_ϕ/(m^3·mol^{-1}·Pa^{-1})	V_ϕ/(kg·m^{-3})	k_ϕ/(m^3·mol^{-1}·Pa^{-1})
v_0 or k_0	91.1941	−402.241	94.8636	−553.165
v_1 or k_1	0.18671	2.38501	0.22855	3.26581
v_2 or k_2	$-1.1201\cdot10^{-4}$	$-3.5350\cdot10^{-3}$	$-9.8796\cdot10^{-5}$	$-4.8081\cdot10^{-3}$
a_0	15.8086	188.341	23.9278	79.9132
a_1	$-9.7880\cdot10^{-3}$	−1.17784	$-3.5272\cdot10^{-2}$	−0.46819
a_2		$1.8369\cdot10^{-3}$		$6.2696\cdot10^{-4}$
b_0	−9.27719	69.1187	−13.999	556.216
b_1	$5.7379\cdot10^{-3}$	−0.37443	$2.0635\cdot10^{-2}$	−3.31499
b_2	$1.0168\cdot10^{-8}$	$5.1364\cdot10^{-4}$	$1.0973\cdot10^{-9}$	$5.0124\cdot10^{-3}$
c_0	−0.34446	−5.6116	−0.34229	7.7164
c_1	$-5.3013\cdot10^{-8}$	0.039783	$-7.1439\cdot10^{-9}$	$-4.5456\cdot10^{-2}$
c_2		$-6.7081\cdot10^{-5}$		$7.6178\cdot10^{-5}$
σ	0.25	0.17	0.24	0.18

TABLE 7
Pitzer–Simonson parameters $U^V_{s,MX}$, $W^V_{s,MX}$ and $\overline{V^0_\phi}$ of equation (12), for the ammonium ILs in water, and limiting apparent molar volume, V^0_ϕ of equation (10) at several temperatures.

T/K	V^0_ϕ/(cm^3·mol^{-1})	$\overline{V^0_\phi}$/(cm^3·mol^{-1})	$10^3U^V_{s,MX}$/(MPa^{-1})	$10^3W^V_{s,MX}$/(MPa^{-1})	σ/(cm^3·mol^{-1})
			m2HEAB(1) + H_2O(2)		
298.15	136.903	142.741	2.7573	−2.2309	1.0
303.15	137.500	143.494	2.5661	−2.1335	1.0
308.15	138.091	144.158	2.4154	−2.0521	1.0
313.15	138.677	144.747	2.2990	−1.9841	1.0
318.15	139.257	145.255	2.2170	−1.9298	1.0
323.15	139.831	145.693	2.1635	−1.8866	1.0
328.15	140.400	146.063	2.1360	−1.8537	1.0
333.15	140.963	146.370	2.1319	−1.8300	1.0
			m2HEAP(1) + H_2O(2)		
298.15	154.223	160.616	2.7048	−2.3142	0.9
303.15	155.069	161.849	2.2898	−2.1560	0.8
308.15	155.910	163.000	1.9198	−2.0150	0.7
313.15	156.746	164.081	1.5880	−1.8888	0.7
318.15	157.577	165.087	1.2946	−1.7773	0.6
323.15	158.403	166.028	1.0332	−1.6781	0.6
328.15	159.224	166.908	8.0125	−1.5902	0.5
333.15	160.040	167.730	5.9607	−1.5125	0.5

The properties needed for calculation of values of A^V_x and b values are given as supporting information (see table S2). Values of partial molar volumes $\overline{V^0_\phi}$ and the parameters $W^V_{s,MX}$ and $U^V_{s,MX}$ are given in table 7 for the essayed temperatures. In the same table, the limiting partial molar volumes $\overline{V^0_\phi}$ derived from equation (15) are compared with V^0_ϕ obtained from equation (10). The limiting apparent molar volume values obtained from the rational function equation (10) are lower by about (6 to 8) cm^3·mol^{-1} than the partial molar volumes resulting from the Pitzer–Simonson equation. The temperature dependence of the limiting apparent molar volume values given by equation (10) is: V^0_ϕ/(cm^3·mol^{-1}) = 91.1941 + 0.186705 (T/K) − $1.1201\cdot10^{-4}$ (T/K)^2 for m2HEAB and V^0_ϕ/(cm^3·mol^{-1}) = 94.8636 + 0.22855 (T/K) − $9.87959\cdot10^{-5}$ (T/K)^2 for m2HEAP. The partial molar volumes calculated from the Pitzer–Simonson equation were fitted to a quadratic polynomial in temperature: $\overline{V^0_\phi}$/(cm^3·mol^{-1}) = −36.5538 + 1.04718 (T/K) − $1.4952\cdot10^{-3}$ (T/K)^2 and $\overline{V^0_\phi}$/(cm^3·mol^{-1}) = −35.347 + 1.06406 (T/K) − $1.3643\cdot10^{-3}$ (T/K)^2 for m2HEAB and m2HEAP, respectively. Therefore, the limiting apparent molar volume expansibility, $\alpha^0_p = (\partial V^0_\phi/\partial T)_p$ or $\alpha^0_p = (\partial \bar{V}^0_\phi/\partial T)_p$ is positive and decreases very slowly with temperature. It can be seen that α^0_p resulting from equation (10) remains constant at about 0.12 cm^3·mol^{-1}·K^{-1} and 0.17 cm^3·mol^{-1}·K^{-1} for the two ILs over the range of temperatures studied. Following Zafarani-Moattar *et al.* [31], positive expansibility is a characteristic property of aqueous solutions with hydrophobic hydration and this behaviour means electrostriction of electrolytes in aqueous solutions. On heating, some water molecules can be released from the hydration layers [32] which increase the solution volume. High positive values of α^0_p have been observed for aqueous solutions of imidazolium-based ILs [31] whereas negative values are observed for alcoholic mixtures of ILs [32]. According to Hepler [33], the sign of $(\partial\alpha^0_p/\partial T)_p = (\partial^2\bar{V}^0_\phi/\partial T^2)_p$ provides a qualitative criterion for the characterisation of the long-range structure-making or -breaking ability of a solute in solution. A positive sign or close to zero value of $(\partial^2\bar{V}^0_\phi/\partial T^2)_p$ indicates a structure maker solute, otherwise is a structure breaker. The expressions mentioned before show that $(\partial^2\bar{V}^0_\phi/\partial T^2)_p$ values are negative, indicating that the ammonium ILs studied act as structure breaker in water which in turn form chains around the IL molecules. This behaviour agrees with MD results [23] indicating that for water mole fractions in the range (0.8 to 0.9) the average number of neighbours of a given water molecule is lowered from (∼5) found in bulk water aggregates [34] to 2 or 3.

3.3. Acoustical properties

The speed of sound for pure m2HEAB and m2HEAP at atmospheric pressure was measured over the temperature range T = (293.15 to 343.15) K and the results are presented in table 2 and plotted in figure 5. The results for m2HEAPr, reported in this authoŕs previous study [12], are also plotted for comparison. In this figure, those values are compared with results reported by Álvarez *et al.* [21]. The measured values presented by them are always significantly higher than the ones reported in this study. Deviations are from (3 to 4)% at T = (293.15 and 338.15) K, respectively, for m2HEAPr and m2HEAB (about 60 m·s^{-1}) and 2% (about 30 m·s^{-1}) for m2HEAP. These significant differences can be accounted due to water contamination and possibly the different measurement techniques used. The ILs samples measured by Álvarez *et al.* were dried for 48 h at ambient temperature under a medium vacuum (of 20 kPa) with stirring before each use but the water content in the ILs was not measured because the room humidity was not completely controlled. The contamination with water of the ammoniums used by Álvarez *et al.* could be a major problem in the measurements because as table 3 shows, small water quantities increase speed of sound of N-methyl-2-hydroxyethylammoniums. Taking for example our data for m2HEAB for the aqueous mixture with x_{IL} = 0.8 and the pure IL, assuming that our results are more feasible and that linear behaviour between speed of sound and mole fraction holds within this range, it can be concluded that the sample studied by Alvarez *et al.* could contain up to 0.02 mass fraction of water. Probably m2HEAP was the less water contaminated IL.

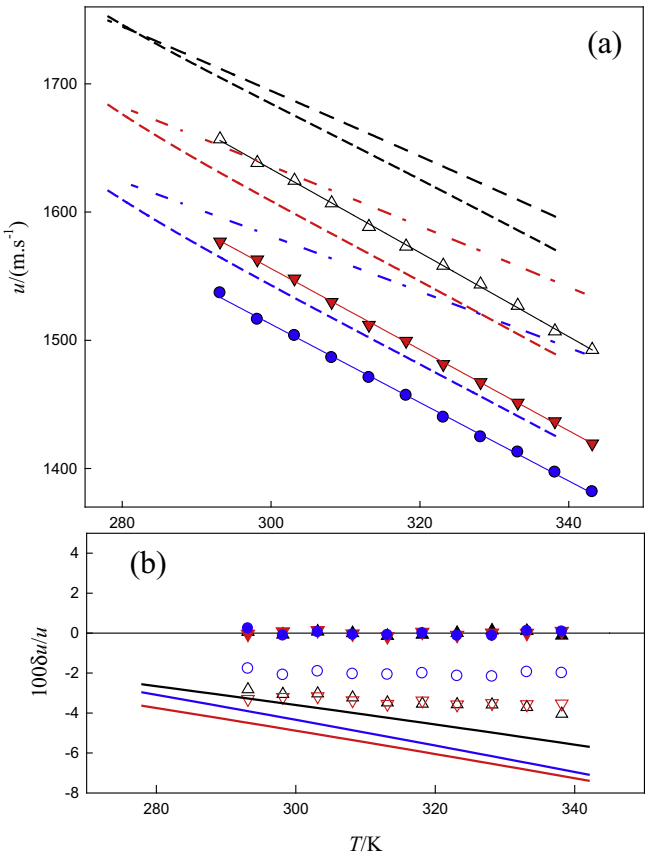

FIGURE 5. (a) Speed of sound, u, of m2HEAPr, m2HEAB and m2HEAP as a function of temperature. Experimental values: Δ, m2HEAPr [12]; ▼, m2HEAB; ●, m2HEAP; solid lines, correlation with equation (16); dashed lines, Álvarez *et al.* [21]; dash-dot lines, prediction with Wu *et al.* method [38]. (b) Relative deviations of experimental values from data measured by Álvarez *et al.* [21]: Δ, m2HEAPr [12]; ▽, m2HEAB (this work); ○, m2HEAP (this work); relative deviations of experimental values from equation (16): ▲, m2HEAPr [12]; ▼, m2HEAB; ●, m2HEAP; Solid lines refer to the relative deviations of experimental values from predictive Wu *et al.* method: black, m2HEAPr [12]; red, m2HEAB; blue, m2HEAP. (For interpretation of the references to colour in this figure legend, the reader is referred to the web version of this article.)

Values of the speed of sound of this work have also been correlated with temperature using the equation proposed by Rao [35]:

$$u = u_0(1 - T/T_c)^m, \tag{16}$$

where u_0 is the speed of sound at absolute zero, T_c is the critical temperature, m and u_0 are fitting parameters. Rao proposed m = 0.9 and it is interesting to note that the equation (16) is similar to that proposed later by Guggenheim [36] to represent the surface tension variation with temperature. The critical temperature for ionic liquids was obtained by the group contribution method proposed by Valderrama *et al.* [37] and already used in [12]. For m2HEAB and m2HEAP, T_c = (760.26 and 782.49) K, were obtained respectively [38]. The fitting equation (16), by least squares, to the speed of sound given in table 2 gives u_0 = (2484.1 ± 10.5) m·s^{-1}, m = (0.9322 ± 0.0078) with standard deviation σ_u = 1.4 m·s^{-1} for m2HEAB and u_0 = (2421.9 ± 14.6) m·s^{-1}, m = (0.9736 ± 0.0078) and σ_u = 1.9 m·s^{-1} for m2HEAP. Equation (16) is represented in figure 5.

Recently, Wu *et al.* [38] proposed a corresponding states group contribution method for estimating the speed of sound of ILs based on speed of sound data of 96 pure ILs (containing 51 cations and 23 anions) reported between 2005 and 2013. The proposed equation was:

$$u = \sum_{i=0}^{3} a_i \left(\sum_{j=1}^{k} n_j \Delta u_{0_j} \right)^i (1 - T/T_c)^{0.65359}, \tag{17}$$

where n_j is the number of groups of type j, k is the total number of different groups in the ionic fragment, and a_i and Δu_{0j} are parameters and group contribution parameters for group j, respectively. An average absolute deviation (*AAD*) of 2.34% has been obtained for a total of 96 ionic liquids covering imidazolium, pyridinium, pyrrolidinium, phosphonium, and ammonium cations combined with a large variety of anions. In figure 5, the speed of sound values predicted using equation (17) are compared with those reported in this work and those determined by Álvarez *et al.* [21]. It can be concluded that the predicted values from the Wu *et al.* equation are always higher than our values by figures as large as 7% for m2HEAB and m2HEAP at temperatures close to 340 K. Also, the data presented by Álvarez *et al.* [21] are lower than those estimated with the Wu method, although the agreement is better. Wu *et al.* referred that the method cannot provide satisfactory results for protic ILs due to the presence of proton-donor and proton-acceptor sites.

The experimental speed of sound was correlated using the rational function of the form:

$$u = x_1 u_1 + x_2 u_2 + x_1 x_2 \frac{\sum_{i=0}^{m} (C_{i0} + C_{i1} T)(2x_1 - 1)^i}{1 + \sum_{j=1}^{n} (D_{j0} + D_{j1} T)(2x_1 - 1)^j}. \tag{18}$$

The adjustable coefficients C_{ik} (k = 0, 1) and D_{jk} (k = 0, 1) were obtained by fitting equation (18) to the variations $\Delta u/x_1x_2[\Delta u/x_1x_2 = (u - x_1u_1 - x_2u_2)/(x_1x_2)]$ using simultaneously the temperature and composition over the whole ranges and are presented in table 4 for the aqueous mixtures of m2HEAB and m2HEAP. The aforementioned variations show characteristic hyperbolic shapes with a step increase observed near x_1 = 0, as shown in figure 6. From table 4 it can be concluded that the correlation of speed of sound with equation (18) is reasonable for the whole temperature and composition ranges as revealed by standard deviations (7.3 and 3.3) m·s^{-1} with corresponding average

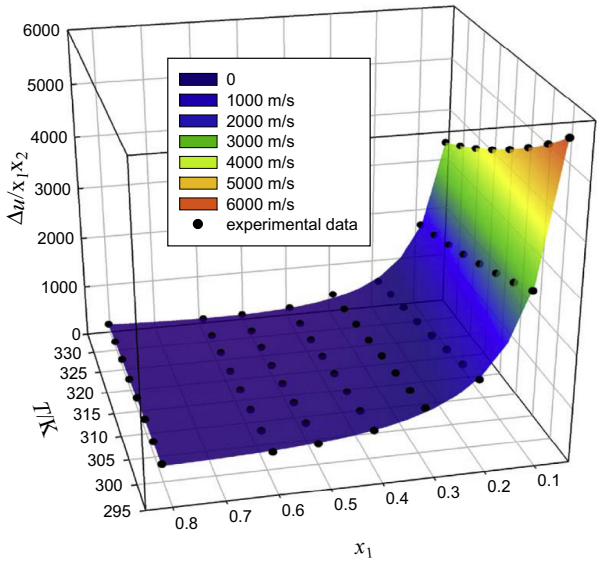

FIGURE 6. Surface plot of function $\Delta u/x_1x_2$ versus mole fraction of ionic liquid, x_1, and temperature for m2HEAB. The coloured surface represents the fitted values to equation (18). (For interpretation of the references to colour in this figure legend, the reader is referred to the web version of this article.)

absolute deviations (0.31 and 0.16)%. Standard deviations in speed of sound ranging from (1.5 to 8.5) m·s^{-1} were reported by Alvarez *et al.* [13], who used polynomial expressions with 21 coefficients for 2-hydroxyethylammonium acetate (+water, methanol, or ethanol) systems. The relative deviations of the calculated speed of sound values by equation (18) from the experimental ones are presented in figure 7. They are usually lower than 0.5% but important data scatter is observed, presenting the relative deviation large variations even for fixed composition at various temperatures (for example for (m2HEAB(1) + H_2O(2)) at $x_1 = 0.1960$ the deviations range between (0.3 to 0.7)%). Most likely factors as heterogeneous mixing and temperature can influence the speed of sound measurement for the mixtures and the resulting uncertainty will be higher than the combined uncertainty obtained from cell calibration (±1.2 m·s^{-1}). Considering that equation (18) represents a standard behaviour to which corresponds the minimum error, the expected uncertainty will be of the order of the standard deviation. For each of the aqueous m2HEAB and m2HEAP systems, it is found that only a very small number of mixtures show absolute deviations in the speed of sound with values higher than the

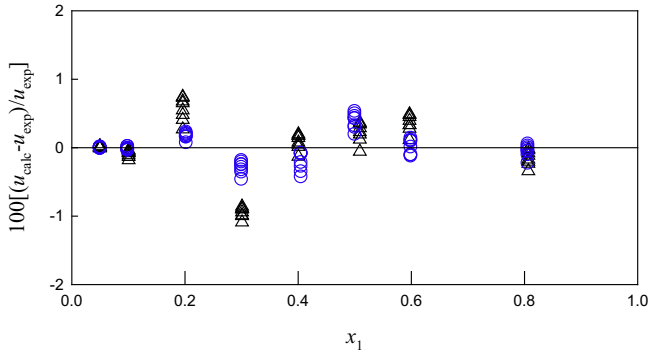

FIGURE 7. Relative deviations between the calculated speed of sound values (u_{calc}) with correlation equation (18) and experimental values (u_{exp}), for the aqueous mixtures of ILs as function of x_1 and temperature: Δ, {m2HEAB(1) + H_2O(2)}; ○, {m2HEAP(1) + H_2O(2)}.

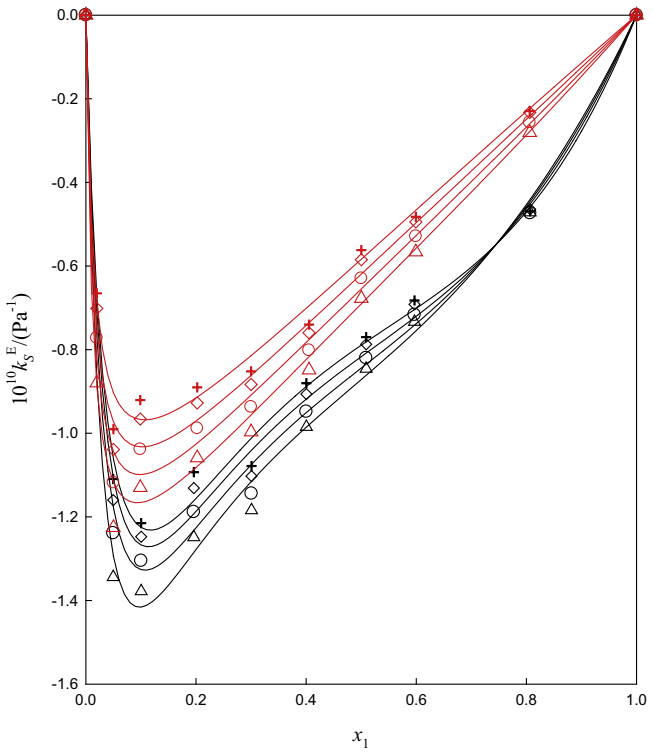

FIGURE 8. Excess isentropic compressibility, k_S^E *versus* mole fraction, x_1, and temperature. Δ, 298.15 K; ○, 308.15 K; ◇, 318.15 K; +, 328.15 K, for {m2HEAB(1) + H_2O(2)} (black) and {m2HEAP(1) + H_2O(2)} (red). Solid curves were calculated from equation (20). (For interpretation of the references to colour in this figure legend, the reader is referred to the web version of this article.)

respective standard deviation. This reasoning allows setting a maximum uncertainty of speed of sound of the order of ±7 m·s^{-1} for the measurements in the aqueous ILs systems.

Speed of sound measurements of aqueous electrolyte solutions provides information about ion–ion and ion–solvent interactions [39]. Based on the measured speed of sound and density values, reported in table 3, the isentropic compressibility of the mixture, k_S, was calculated from the Laplace–Newtońs equation $k_S = (1/\rho u^2)$. The uncertainty in k_S, $u(k_S)$, was calculated from the errors propagation method using the standard deviations obtained for the experimental density and speed of sound. A maximum uncertainty of the order ±6.0 10^{-13} Pa^{-1} was found. The excess isentropic compressibility $k_S^E = k_S - k_S^{id}$, was calculated using the rigorous thermodynamic ideal-mixing rule for isentropic compressibility, k_S^{id}, found by Benson and Kiyohara [40] and discussed by Douhéret *et al.* [41]:

$$k_S^{id} = \sum_{i=1}^{2}\phi_i k_{S,i} + T\left[\sum_{i=1}^{2}\frac{\phi_i V_{m,i}\alpha_{p,i}^2}{C_{p,m,i}} - \frac{V_m^{id}(\alpha_p^{id})^2}{C_{p,m,i}^{id}}\right], \quad (19)$$

where $\phi_i\,(= x_i V_{m,i}/V_m^{id})$ is the volume fraction of the component i in the mixture, whereas $\alpha_{p,i}$ and $C_{p,m,i}$ are the thermal expansivity and molar heat capacity, respectively, of pure component i. The $V_m^{id}\,(= \sum_i^2 x_i V_{m,i})$, $\alpha_p^{id}\,(= \sum_i^2 \phi_i \alpha_{p,i})$ and $C_{p,m}^{id}\,(= \sum_i^2 x_i C_{p,i})$ are the molar volume, thermal expansivity and molar isobaric heat capacity, respectively, of the ideal mixture. All the above properties values as well as the k_S, k_S^{id}, and k_S^E are provided in table S1, in supplementary information. The k_S^E values were correlated with the IL mole fraction by the rational function:

$$k_S^E = x_1 x_2 \frac{\sum_{i=0}^{m}(A_{i0} + A_{i1}T)(2x_1 - 1)^i}{1 + \sum_{j=1}^{n}(B_{j0} + B_{j1}T)(2x_1 - 1)^j}. \quad (20)$$

The correlation coefficients A_{ik} and B_{jk} ($k = 0, 1$) are given in table 5 with the corresponding standard deviations $\sigma(k_S)$. In figure 8 the experimental and the calculated values of k_S^E from equation (20) are displayed for the binary systems (m2HEAB + H_2O) and (m2HEAP + H_2O) as a function of the IL mole fraction and temperature. The corresponding surface plot for (m2HEAB + H_2O) is given in figure S2 as supplementary material. The excess isentropic compressibility is always negative for the whole range of temperatures and compositions and becomes less negative when the temperature increases. The k_S^E curves are remarkably asymmetric, with sharp minima at low values of IL mole fraction ($x_1 \approx 0.1$). The high negative values of the (IL + H_2O) mixtures are due to the closer proximity between water molecules and IL ions, and the strong interaction between them, leading to a compressibility decreasing. This fact is in agreement with the MD results [23] as discussed before in the volumetric part of this work.

Douhéret *et al.* [41] stated that the speed of sound in an ideal-mixture u^{id} may be obtained with equation (21):

$$u^{id} = \left(\rho^{id} k_S^{id}\right)^{-1/2} = \left(\frac{V_m^{id}}{k_S^{id} M}\right)^{1/2}, \quad (21)$$

allowing the excess speed u^E (=$u - u^{id}$) calculation. The values of u^{id} and u^E are given in table S1. The u^E values were correlated by rational functions (analytically similar to equation (20)), and the coefficients and standard deviation $\sigma(u^E)$ are given in table 5. The experimental and correlated values of u^E with equation (20) are represented in figure 9 for the systems (m2HEAB + H_2O) and (m2HEAP + H_2O). The surfaces u^E–x_1–T are plotted in figures S3 and S4 for m2HEAB and m2HEAP.

Similar to that observed in the previous work, for (m2HEAPr + H_2O) [12], the u^E is always positive over the whole range of temperature and compositions, but it decreases with the temperature increase. The fitted curves are very asymmetric, presenting a maximum at the low IL mole fraction ($x_1 \approx 0.1$) similar to what can be observed for k_S^E. The excess speed of sound and the excess isentropic compressibility are closely related. It can be shown [12] that

$$u^E = \frac{1}{\rho^{1/2}(k_S^E + k_S^{id})^{1/2}} - \frac{1}{\rho_{id}^{1/2}(k_S^{id})^{1/2}}. \quad (22)$$

Furthermore, subtraction of term $1/\rho_{id}^{1/2}\left(k_S^{id}\right)^{1/2}$ from $1/\rho^{1/2}\left(k_S^E + k_S^{id}\right)^{1/2}$ will withdraw influence of k_S^{id} and then evidencing more the analytical influence of k_S^E in u^E. The almost symmetrical shape observed in figures 8 and 9 can be explained in this way.

The apparent IL molar isentropic compressibility values, k_ϕ, of the ionic liquid aqueous mixtures were computed using equation (23):

$$k_\phi = \frac{k_S M_1}{\rho} + \frac{(k_S \rho_2 - k_{S,2}\rho)}{m\rho_2\rho}, \quad (23)$$

where $k_{S,2}$ and k_S are the water and the binary mixture (IL + water) isentropic compressibility, respectively. The uncertainties in k_ϕ, $u(k_\phi)$, are of the order of $\pm 5.4 \times 10^{-16}$ $m^3 \cdot mol^{-1} \cdot Pa^{-1}$ and $\pm 1.0 \times 10^{-16}$ $m^3 \cdot mol^{-1} \cdot Pa^{-1}$ at low and high concentrations of ionic liquid, respectively. The calculated apparent molar compressibility from equation (23) are given in table S1 and plotted in figure 10

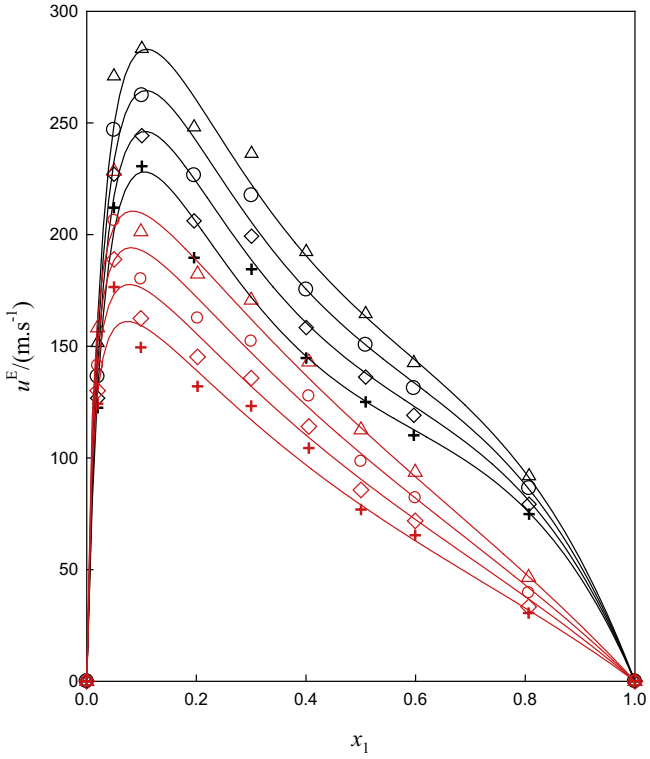

FIGURE 9. Excess speed of sound, u^E as a function of mole fraction, x_1 at several temperatures. Δ, 298.15 K; ○, 308.15 K; ◇, 318.15 K; +, 328.15 K, for {m2HEAB(1) + H_2O(2)} (black) and for {m2HEAP(1) + H_2O(2)} (red). Solid curves were calculated from equation (20) for u^E. (For interpretation of the references to colour in this figure legend, the reader is referred to the web version of this article.)

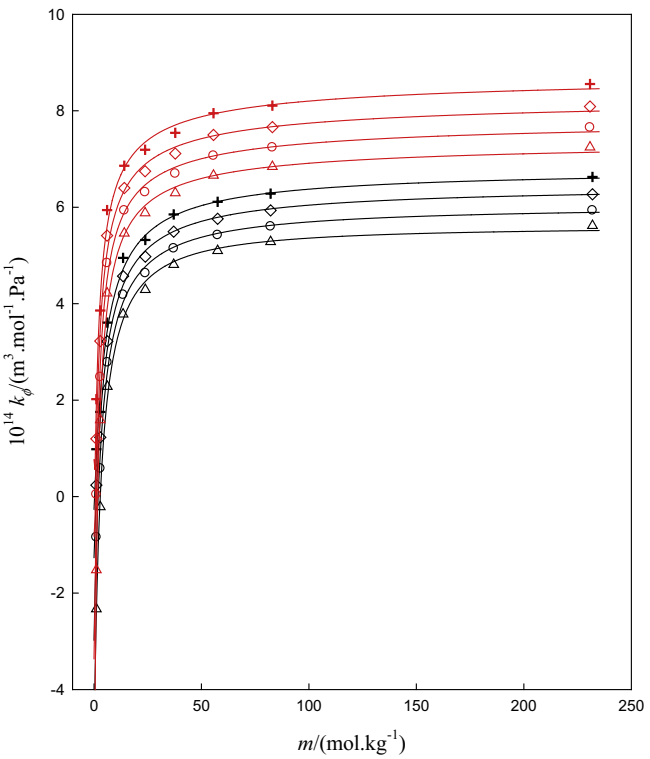

FIGURE 10. Apparent molar isentropic compressibility, k_ϕ, versus molality, m, at several temperatures for {m2HEAB(1) + H_2O(2)} (black) and {m2HEAP(1) + H_2O(2)} (red): Δ, 298.15 K; ○, 308.15 K; ◇, 318.15 K; +, 328.15 K. Solid curves were calculated from equation (24). (For interpretation of the references to colour in this figure legend, the reader is referred to the web version of this article.)

as function of the IL molality and temperature. The apparent molar compressibility increases rapidly up to molality of $m \approx 25$ kg·mol^{-1} and it becomes almost constant afterwards that is also a behaviour verified for the apparent molar volume.

The apparent molar isentropic compressibility is also well described by rational functions:

$$k_\phi = k_\phi^0(T) + \frac{A_k(T)(m)^{1/2} + B_k(T)m}{1 + C_k(T)m}, \quad (24)$$

where $k_\phi^0 = k_0 + k_1T + k_2T^2$, $A_k(T) = a_0 + a_1T + a_2T^2$, $B_k(T) = b_0 + b_1T + b_2T^2$, $C_k(T) = c_0 + c_1T + c_2T^2$. From least squares, the parameters (corresponding to $10^{14}k_\phi$) k_i, a_i, b_i and c_i are listed in table 6. For dilute IL solutions when $(m \to 0)$, equation (24) leads to equation proposed by Dey *et al.* [42]:

$$k_\phi = k_\phi^0 + A_k(m)^{1/2} + B_k m, \quad (25)$$

where A_k is the Debye–Hückel limiting slope for apparent molar isentropic compressibility, and the slope B_k is an empirical constant obtained by fitting of equation (25) to apparent molar isentropic compressibility data.

The k_ϕ values calculated from equation (24) are represented in figure 10 and the surfaces k_ϕ–m–T are illustrated in figures S5 and S6. For values of molality up to 25 kg·mol^{-1}, k_ϕ increases exponentially (k_ϕ values around 6 m^3·mol^{-1}·Pa^{-1}) followed by an almost constant regime afterwards. The k_ϕ–m–T behaviour is similar to that observed in the system (m2HEAPr + H_2O) [12].

As the limiting apparent molar volumes, the limiting molar apparent compressibility, k_ϕ^0, $(k_\phi(x_{IL} \to 0))$, gives the extent of ion–solvent interactions. The k_ϕ^0 values are appreciably negative for the ILs studied here, especially at lower temperatures, indicating that these ILs lead to an electrostriction effect, which means an appreciable decrease in the mixture compressibility. The main factors contributing to the k_ϕ^0 values are the ions intrinsic compressibility (usually a positive contribution), and the penetration of the solvent molecules in the free volume of the ionic solute (negative contribution). Therefore the significant negative k_ϕ^0 will be due to the predominance of water penetration compared with the compressibility of the ionic species. Zhao *et al.* [43] referred that ILs dilute solutions can form oligomeric aggregates between cations and anions with free volume depending on the solution concentration. This situation will cause penetration of small water molecules in the intra-ionic free space. Furthermore, Álvarez *et al.* [13] studied the aggregation, dynamic behaviour and hydrogen-bond network of aqueous mixtures of 2HEAA by thermo-acoustical, X-ray, and nuclear magnetic resonance techniques. They concluded that a water structure around the ($-NH_3^+$) species exists at different water mole fractions reflecting the transient formation of a complex with a long life between 2HEAA and one or more water molecules.

In the work by the authors [12], the molar compressibility values or Wadás constant [44] of pure m2HEAPr and its aqueous mixtures were calculated as:

$$k_m = \frac{M}{\rho} k_S^{-1/7}. \quad (26)$$

The results for molar compressibility of pure m2HEAB, 2HEAP and water as well for the ILs aqueous mixtures are presented in table S1 as supplementary information. The uncertainties in the calculation of k_m, $u(k_m)$, can be estimated as $\pm(3.0 \times 10^{-7}$ and $7.0 \times 10^{-7})$ m^3·mol^{-1}·Pa$^{1/7}$ at low and high concentrations of ionic liquid, respectively. In figure 11, the molar compressibility is plotted versus temperature for fixed compositions. It is observed that k_m is an almost a constant function of temperature as seen before [12] for pure m2HEAPr, pure water and (m2HEAPr + H_2O) mixtures. Observing figure 11(a) and (b) and from table 8 it can

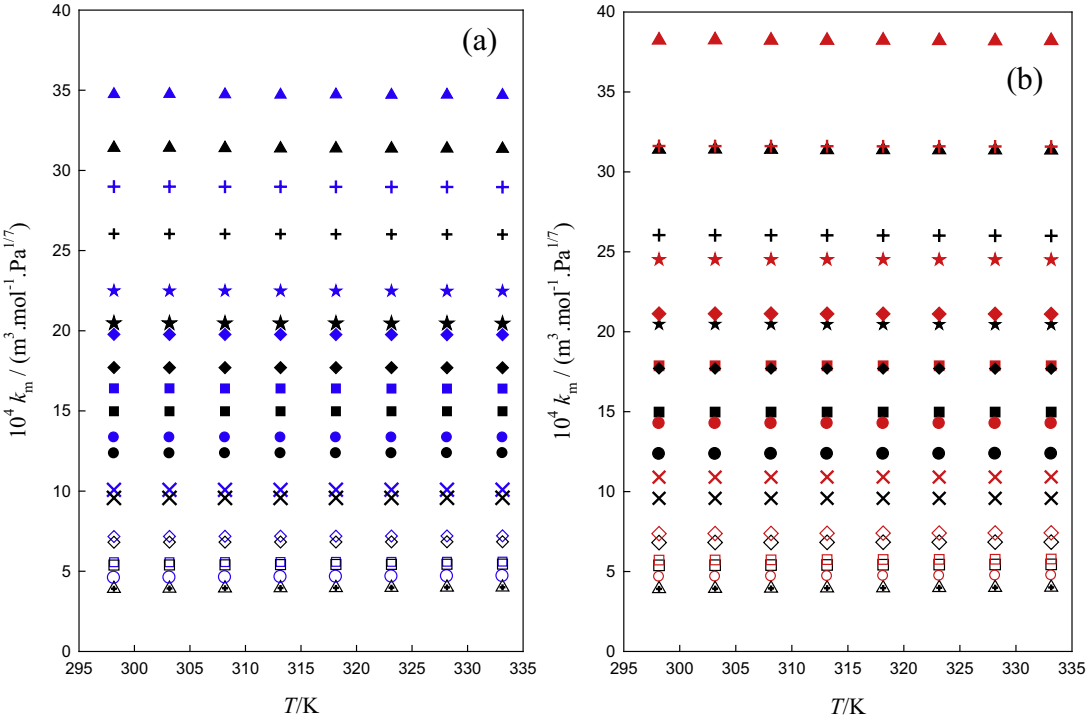

FIGURE 11. Molar compressibility of aqueous solutions, k_m, as a function of temperature and mole fraction of IL at approximate mole fractions (◬), $x_1 = 0$; (○), $x_1 = 0.02$; (□), $x_1 = 0.05$; (◇), $x_1 = 0.1$; (×), $x_1 = 0.2$; ●, $x_1 = 0.3$; (■), $x_1 = 0.4$; (◆), $x_1 = 0.5$; (★), $x_1 = 0.6$; (+) $x_1 = 0.8$, (▲), $x_1 = 1.000$ for: (a) {m2HEAPr(1) + H_2O(2)} (black) and {m2HEAB(1) + H_2O(2)} (blue); (b) {m2HEAPr(1) + H_2O(2)} (black) and {m2HEAP(1) + H_2O(2)} (red). For isomole fraction the range of temperature is (298.15 to 333.15) K at 5 K intervals. (For interpretation of the references to colour in this figure legend, the reader is referred to the web version of this article.)

TABLE 8
Mean molar compressibility $\langle k_m \rangle$, standard deviation, σ_{km}, and average relative deviation, *AAD*, from the mean molar compressibility versus mole fraction for the aqueous mixtures of N-methyl-2hydroxyethylammonium ILs.

x_1	$10^4 \cdot \langle k_m \rangle / (m^3 \cdot mol^{-1} \cdot Pa^{1/7})$	$10^4 \cdot \sigma_{km} / (m^3 \cdot mol^{-1} \cdot Pa^{1/7})$	*AAD*%
	m2HEAPr[a]		
0.0000	3.9582	0.0287	0.631
0.0200	4.5676	0.035	0.660
0.0501	5.4158	0.019	0.306
0.1001	6.8250	0.010	0.128
0.1010	6.8505	0.010	0.131
0.2006	9.5765	$9.7 \cdot 10^{-4}$	0.009
0.3010	12.3536	$4.3 \cdot 10^{-3}$	0.030
0.3978	14.9763	$5.0 \cdot 10^{-4}$	0.003
0.4976	17.6984	$3.5 \cdot 10^{-3}$	0.017
0.5972	20.4607	$6.6 \cdot 10^{-3}$	0.028
0.8006	26.0244	0.015	0.049
1.0000	31.3776	0.021	0.060
	m2HEAB		
0.0000	3.9583	0.0287	0.631
0.0199	4.6417	0.0362	0.680
0.0497	5.5797	0.0119	0.186
0.1005	7.1861	0.0136	0.166
0.1960	10.0810	$3.0296 \cdot 10^{-3}$	0.026
0.3008	13.3371	$4.9255 \cdot 10^{-4}$	0.003
0.4005	16.4001	$5.3283 \cdot 10^{-3}$	0.028
0.5090	19.7619	$7.0314 \cdot 10^{-3}$	0.031
0.5968	22.4827	$7.0999 \cdot 10^{-3}$	0.027
0.8069	28.9745	0.0106	0.032
1.0000	34.7232	0.0204	0.052
	m2HEAP		
0.0000	3.9583	0.0287	0.631
0.0199	4.7093	0.0303	0.561
0.0500	5.7473	0.0214	0.325
0.0988	7.3954	0.0164	0.194
0.2023	10.9078	$4.4266 \cdot 10^{-3}$	0.035
0.3000	14.2643	$8.9186 \cdot 10^{-4}$	0.005
0.4053	17.8734	$7.0094 \cdot 10^{-4}$	0.003
0.5003	21.1183	$6.3546 \cdot 10^{-3}$	0.026
0.5993	24.5136	$4.8462 \cdot 10^{-3}$	0.017
0.8061	31.6022	0.0131	0.036
1.0000	38.2222	0.0177	0.039

[a] From [12].

be concluded that the inclusion of a (-CH_2-) group in the anionic hydrocarbon chain gives an increase of a maximum of 3×0^{-4} $m^3 \cdot mol^{-1} \cdot Pa^{1/7}$ (near 10%) in k_m, for the mixtures with $x_{IL} > 0.5$. In the previous work [12], the calculations showed that k_m was a so weak function on temperature that in the representation $k_m = k_1 + k_2 T + k_3 T^2$, the temperature dependent terms contribution was less than 2% except for water and the IL dilute solutions ($x_1 \leqslant 0.1$). The same was verified for m2HEAB and m2HEAP and their aqueous mixtures. For this reason, k_m was averaged on temperature for each mole fraction and the mean values $\langle k_m \rangle = (1/N_p) \sum_i^{N_p} (k_m)_i$ ($N_p = 8$) were calculated as before [12]. These results are presented in table 8 as well as the standard deviation from the mean value of molar compressibility, σ_{km}, and the average absolute deviation from the mean, *AAD* defined respectively, by equations (27) and (28):

$$\sigma_{km} = \left[\sum_{i=1}^{N_p} (k_m - \langle k_m \rangle)_i^2 / N_p \right]^{1/2}, \tag{27}$$

$$AAD\% = (100/N_p) \sum_{i=1}^{N_p} |(k_m - \langle k_m \rangle) / \langle k_m \rangle|_i. \tag{28}$$

In table 8, the values given for (m2HEAPr + H_2O) mixtures [12] are included for comparison. The standard deviation σ_{km} is usually

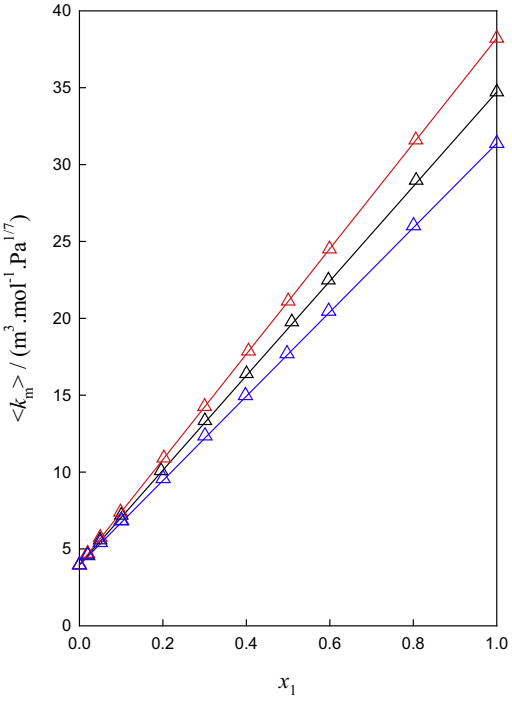

FIGURE 12. Mean compressibility (temperature averaged) versus mole fraction of IL: {m2HEAPr(1) + H_2O(2)} (blue), {m2HEAB(1) + H_2O(2)} (black), and {m2HEAP(1) + H_2O(2)} (red). Lines refer to the "ideal" behaviour. (For interpretation of the references to colour in this figure legend, the reader is referred to the web version of this article.)

lower than 1×10^{-6} $m^3 \cdot mol^{-1} \cdot Pa^{1/7}$ or it reaches this order of magnitude and the *AAD*% is lower than 0.05%, except for water and the IL dilute solutions. For the aqueous mixtures of m2HEAB and m2HEAP, $\langle k_m \rangle$ is a function nearly linear on mole fraction of IL as shown in figure 12 where the "ideal" behaviour given by $\langle k_m \rangle^* = x_1 \langle k_m \rangle_1 + x_2 \langle k_m \rangle_2$, connecting the pure liquid mean molar compressibility ($\langle k_m \rangle_1$ and $\langle k_m \rangle_2$), was plotted.

Knowing the molar compressibility of the pure compounds, the speed of sound of their mixtures can be predicted, at any temperature and composition, using the equation (26). As the values of k_m are available for the aqueous mixtures of hydroxyethylammoniums we may ask if the prediction of the speed of sound is possible from equation (26) at any temperature and composition in the studied ranges and using the simple assumption $k_m = \langle k_m \rangle^*$. From equation (26) with this assumption:

$$u = (\langle k_m \rangle^* / M)^{7/2} \times \rho^3. \tag{29}$$

The experimental and predicted values of u are represented in the parity plot of figure 13. With the exception of pure water and very dilute IL solutions ($x_1 = 0.02$), the deviations between the calculated and experimental u values of the m2HEAB and m2HEAP aqueous solutions are lower than 1%. The higher deviations for pure water and dilute aqueous solutions of IL at some temperatures are consequence of significant differences between k_m and the averaged value $\langle k_m \rangle^*$. The m2HEAPr aqueous mixtures give estimates of speed of sound also inside the ±1% limits for the concentrated solutions. However, the major part of values show deviations in the range (2 to 5)%. The authors believe that equation (29) could play an important role for future development of speed of sound correlation and prediction methods in pure ILs and their mixtures with water and other solvents.

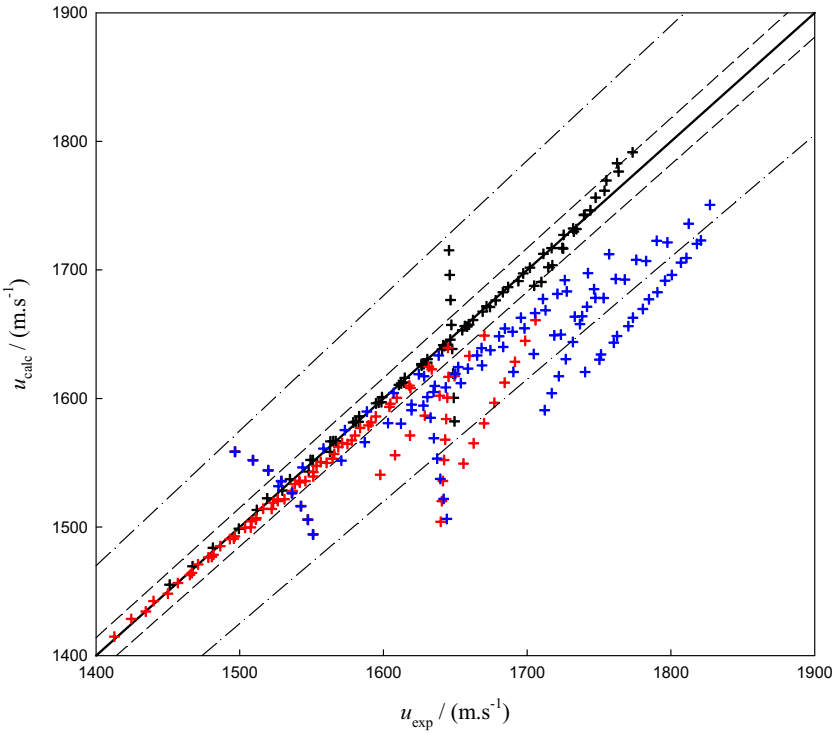

FIGURE 13. Parity plot showing the distribution of experimental and calculated values of the speed of sound for {m2HEAPr(1) + H_2O(2)} (blue), {m2HEAB(1) + H_2O(2)} (black), and m2HEAP(1) + H_2O(2) (red). Dashed lines refer to ±1% deviation and dash-dot lines represent ±5% deviation. (For interpretation of the references to colour in this figure legend, the reader is referred to the web version of this article.)

4. Conclusions

The speed of sound of pure PILs measured in this study at atmospheric pressure compared with the existent values in the literature are (3 to 4)% lower for m2HEAB and 2% lower for m2HEAP. The Wu *et al.* equation predicted speed of sound values with deviations between (4 and 7)%.

The excess molar volume, excess isentropic compressibility, molar compressibility, apparent molar volume and apparent molar isentropic compressibility for the binary mixtures (PIL + water) were calculated from the measured density and speed of sound at temperatures within the (298.15 to 333.15) K temperature range and over the whole composition range.

The analytical representation of (PIL + water) mixtures density can be obtained with good accuracy with rational functions on temperature and IL mole fraction. For all the studied systems, V_m^E and k_S^E show appreciable negative values. The binary V_m^E values were correlated successfully by using Redlich–Kister polynomials with only 3 coefficients. For correlation of the binary k_S^E and u^E the use of rational functions were preferred. The k_S^E curves versus mole fraction show a remarkable asymmetry, with their minima toward to the rich compositions in water. This behaviour indicates the presence of ion–dipole interactions and packing between water and ionic liquid.

The high positive values of the limiting apparent molar volumes or the high partial molar volumes of IL at infinite dilution derived from the Pitzer–Simonson theory indicate appreciable ion–water interactions when the IL is added to water with possible hydrogen bonding between water and methyl-hydroxyethyl ammonium cation. This behaviour is reinforced by the negative values of the apparent molar isentropic compressibility at lower temperatures indicating that in aqueous mixtures there will be important penetration of water in the ionic structure. This behaviour is supported by MD studies indicating that for dilute solutions of IL the average number of neighbours of a given water molecule decreases appreciably and that the IL polar network becomes more fragmented being possible the existence of a water–anion network formed by alternating anions and water molecules.

For the (IL + water) mixtures, the molar compressibility calculated from Wadás model is almost a linear function of mole fraction and can be considered as temperature independent for a fixed mole fraction in the whole composition range. This behaviour allows reasonable prediction of speed of sound in (IL + water) mixtures for a wide temperature and composition range and within ±1% deviation. The necessary values to for predict the of speed of sound are the from the ionic liquid and water molar compressibility. More research must be done in this issue to develop consistent prediction models.

Acknowledgments

This research is sponsored by FEDER funds through the program COMPETE –Operational Programme for Competitiveness Factors – and by national funds through FCT – Foundation for the Science and Technology, under the project PEst-C/EME/UI0285/2013. P.J. Carvalho acknowledges FCT for their post-doctoral grant SFRH/BPD/82264/2011. S. Mattedi acknowledges CNPq/MCT/Brazil (Grant 306560/2013-5 and project 455773/2012-2).

Appendix A. Supplementary data

Supplementary data associated with this article can be found, in the online version, at http://dx.doi.org/10.1016/j.jct.2016.01.028.

References

[1] C. Chiappe, M. Malvaldi, C.S. Pomelli, Pure Appl. Chem. 81 (2009) 767–776.
[2] A. Berthod, M.J. Ruiz-Angel, J. Carda-Broch, J. Chromatogr. A 1184 (2008) 6–18.

[3] K.E. Gutowski, G.A. Broker, H.D. Willauer, J.G. Huddleston, R.P. Swatloski, J.D. Holbrey, R.D. Rogers, J. Am. Chem. Soc. 125 (2003) 6632–6633.
[4] Y. Qiao, A.D. Headly, Catalysts 3 (2013) 709–715.
[5] D.F. Hennedy, C.D. Drummond, J. Phys. Chem. B 113 (2009) 5690–5693.
[6] X. Yuan, S. Zhang, J. Liu, X. Lu, Fluid Phase Equilib. 257 (2007) 195–200.
[7] M. Iglesias, A. Torres, R. Gonzalez-Olmos, D. Salvatierra, J. Chem. Thermodyn. 40 (2008) 119–133.
[8] N.M.C. Talavera-Prieto, A.G.M. Ferreira, P.N. Simões, P.J. Carvalho, S. Mattedi, J. A.P. Coutinho, J. Chem. Thermodyn. 68 (2014) 221–234.
[9] J. Sierra, E. Martí, A. Mengíbar, R. González-Olmos, M. Iglesias, R. Cruañas, M.A. Garau, Effect of new ammonium based ionic liquids on soil microbial activity, in: 5th Society of Environmental Toxicology and Chemistry Congress, Sydney, 2008.
[10] L.M. Varela, M. Garcia, F. Sarmiento, D. Attwood, V. Mosquera, J. Chem. Phys. 107 (1997) 6415–6419.
[11] I.B. Malham, P. Letellier, A. Mayaffre, M. Turmine, J. Chem. Thermodyn. 39 (2007) 1132–1143.
[12] Y. Li, E.J.P. Figueiredo, M.J. Santos, N.M.C. Talavera-Prieto, P.J. Carvalho, A.G.M. Ferreira, S. Mattedi, J. Chem. Thermodyn. 88 (2015) 44–60.
[13] V.H. Alvarez, S. Mattedi, M. Martin-Pastor, M. Aznar, M. Iglesias, J. Chem. Thermodyn. 43 (2011) 997–1010.
[14] K.A. Kurnia, M.M. Taib, M.I.A. Mutalib, T. Murugesan, J. Mol. Liq. 159 (2011) 211–219.
[15] K.A. Kurnia, M.I.A. Mutalib, T. Murugesan, B. Ariwahjoedi, J. Solution Chem. 40 (2011) 818–831.
[16] K.A. Kurnia, B. Ariwahjoedi, M.I.A. Mutalib, T. Murugesan, J. Solution Chem. 40 (2011) 470–480.
[17] M.M. Taib, T. Murugesan, J. Chem. Eng. Data 55 (2010) 5910–5913.
[18] K.S. Pitzer, M. Simonson, J. Phys. Chem. 90 (1986) 3005–3009.
[19] C.E. Ferreira, M.C. Talavera-Prieto, I.M.A. Fonseca, A.T.G. Portugal, A.G.M. Ferreira, J. Chem. Thermodyn. 47 (2012) 183–196.
[20] A.F.G. Lopes, M.C. Talavera-Prieto, A.G.M. Ferreira, J.B. Santos, M.J. Santos, A.T. G. Portugal, Fuel 116 (2014) 242–254.
[21] V.H. Álvarez, N. Dosil, R. Gonzalez-Cabaleiro, S. Mattedi, M. Martin-Pastor, M. Iglesias, J.M. Navaza, J. Chem. Eng. Data 55 (2010) 625–632.
[22] W.W. Focke, B. Du Plessis, Ind. Eng. Chem. Res. 43 (2004) 8369–8377.
[23] C.E.S. Bernardes, K. Shimizu, J.N.C. Lopes, J. Phys.: Condens. Matter 27 (2015) 194116 (12pp).
[24] O. Redlich, D.M. Meyer, Chem. Rev. 64 (1964) 221–227.
[25] K.S. Pitzer, in: K.S. Pitzer (Ed.), Activity Coefficients in Electrolyte Solutions, CRC Press, Boca Raton, FL, 1991. revised edition, Chapter 3.
[26] K.S. Pitzer, Rev. Mineral. 17 (1987) 97.
[27] J.-Z. Yang, X.-M. Lu, J.-S. Gui, W.-G. Xu, H.-W. Li, J. Chem. Thermodyn. 37 (2005) 1250–1255.
[28] J.A. Rard, A.M. Wijesinghe, S.L. Clegg, J. Solution Chem. 39 (2010) 1845–1864.
[29] K.S. Pitzer, Thermodynamics, third ed., McGraw-Hill, New York, 1995.
[30] D.G. Archer, P. Wang, J. Phys. Chem. Ref. Data 19 (1990) 371–411.
[31] M.T. Zafarani-Moattar, F. Frouzesh, H.R. Rafiee, Fluid Phase Equilib. 376 (2014) 40–47.
[32] A.V. Orchillés, V. González-Alfaro, P.J. Miguel, E. Vercher, A. Martínez-Andreu, J. Chem. Thermodyn. 38 (2006) 1124–1129.
[33] L.G. Hepler, Can. J. Chem. 47 (1976) 359–367.
[34] C.E.S. Bernardes, M.E. Minas da Piedade, J.N. Canongia Lopes, J. Phys. Chem. B 115 (2011) 2067–2074.
[35] M.R. Rao, J. Chem. Phys. 9 (1941) 682–685.
[36] E.A. Guggenheim, J. Chem. Phys. 13 (1945) 253–261.
[37] J.O. Valderrama, L.A. Forero, R.E. Rojas, Ind. Eng. Chem. Res. 51 (2012) 7838–7844.
[38] K.J. Wu, Q.L. Chen, C.H. He, AIChE J. 60 (2014) 1120–1131.
[39] B. Lal, M. Sahin, E. Ayranci, J. Chem. Thermodyn. 54 (2012) 142–147.
[40] G.C. Benson, O. Kiyohara, J. Chem. Thermodyn. 11 (1979) 1061–1064.
[41] G. Douhéret, M.I. Davis, J.C.R. Reis, M.J. Blandamer, Chem. Phys. Chem. 2 (2001) 148–161.
[42] N.C. Dey, J. Bhuyan, I. Haque, J. Solution Chem. 32 (2003) 547–558.
[43] Y. Zhao, J. Wang, H. Lu, R. Lin, J. Chem. Thermodyn. 36 (2004) 1–6.
[44] Y. Wada, J. Phys. Soc. Japan 4 (1949) 280–283.

JCT 15-773